Alfarama Journal of Basic & Applied Sciences

Faculty of Science Port Said University

https://ajbas.journals.ekb.eg
ajbas@sci.psu.edu.eg
http://sci.psu.edu.eg/en/

October 2025, Volume 6, Issue IV

DOI: 10.21608/ajbas.2025.405510.1270

ISSN 2682-275X

Submitted: 19/07/2025
Accepted: 29/08/2025

Pages: 464 - 479

Timing of the Granite magmatism, Wadi Abu Abid, North Eastern Desert, Egypt

Mohamed A. Gharib[1,*], Mohamed M. Omar[1], Mohammed Zaky El-Bialy[1], Sherif Mansour[1]

[1] Geology Department, Faculty of Science, Port Said University, Port Said 42522, Egypt

***Corresponding author: mohamed.sadek11@sci.psu.edu.eg**

ABSTRACT

Granitic rocks represent a large portion of the Arabian-Nubian Shield (ANS) exposures in the North Eastern Desert (NED). The timing of the magmatic events plays a major role in illustrating the ANS development. In order to evaluate the ANS, it is important to understand their geochronological order. Therefore, we studied calc-alkaline and alkaline granitic samples from Wadi Abu Abid, Gabal Um Anab area, North Eastern Desert, Egypt, to chronologically evaluate the ANS magmatic process in the studied region. The results show ages of the syn-collisional compressional magmatic event for all the analyzed samples. The resulting ages extended from 755 ± 16 Ma to 667 ± 15 Ma, which represents some conflicts with the traditional classification of the granitoids as being either Older syn-collisional calc-alkaline granitoids or Younger post-collisional alkaline granitic rocks. Xenocrysts with pre-ANS ages noted in five zircon grains in two samples, given ages of 2006 ± 85 Ma, 1887 ± 84 Ma, 1616 ± 73 Ma, 1228 ± 73 Ma, and 1227 ± 70 Ma, which suggest a local rework of an older magmatic source.

Keywords: Older granites, North Eastern Desert, magmatic events, Zircon U-Pb dating, Arabian–Nubian Shield.

1. INTRODUCTION

Granitoids are the most common rocks in the Egyptian basement outcrops in the eastern desert and Sinai (e.g., [1], [2]). Nearly half of this exposed area (100,000 square kilometers) is represented by granitic rocks (e.g., [3], [4], [5], [6], [7]). These exposed basements are part of the large Neoproterozoic juvenile tract known as the Arabian-Nubian Shield (ANS) (e.g., [8], [9], [10]), which evolved along three major tectono-magmatic stages known as: (a) the accretion stage of the island arcs and micro-continents (ca. 900 – 800 Ma) (e.g., [11], [12], [13], [14]), (b) the syn-collision stage (ca. 750– 630 Ma) (e.g., [8], [9], [11], [13]), (c) the post-collision stage (ca. 630 – 550 540 Ma) (e.g., [7], [10], [11], [15]). The

Egyptian ANS represents the northern, less metamorphosed extent of the East African Orogeny (EAO), which activated between ca. 900 Ma and 650 Ma (e.g., [8], [9]). The Eastern Desert is tectonically dissected to three parts North, Center, and South Eastern Desert (NED, CED, and SED) each of which has it's own distinctive feature [16]. The NED (which our the main focus) is characterized by the higher Younger Granites ratio than the Older granite unite, that makes it more similar to Sinai in addition to their lack of volcanic activities (e.g., [17]).

The granitoid outcrops in Egypt are traditionally classified into the Older Granites (OG; 800 – 630 Ma), that is characterized by being I-type, syn-collision, and syn-tectonic granites, and the Younger Granites (YG; 630–540 Ma) which is characterized by being A-type, post-collision, and post-tectonic granites (e.g., [6], [39], [1], [2], [16]).

The two granitic suites coexist in the NED (e.g., [4], [18], [19], [20], [21], [22], [22]), with a controversy between the traditional granitic rock classification and the geochronological way. The traditional classification of the granitic rocks that based on the apparent geochemical composition could give a younger age and vice versa in the Younger Granites (e.g., [23]).

With limited geochronological studies on the NED granitoids, this study aims to provide information on the magmatic evolution of the ANS in the NED and also an insight into its constructing history using zircon U-Pb geochronological data provided by the laser ablation–inductively coupled plasma–mass spectrometry (LA-ICP-MS) analytical technique for six granitic samples (Table 1), those samples were collected from Wadi Abu Abid area (Fig. 2).

Fig. 1. Location map for the northern ANS in Egypt. Terms GoS (Gulf of Suze) and GoA (Gulf of Aqaba), the dash red line separates the NED (North Eastern Desert) from the CED (Center Eastern Desert) after Stern & Hedge (1985).

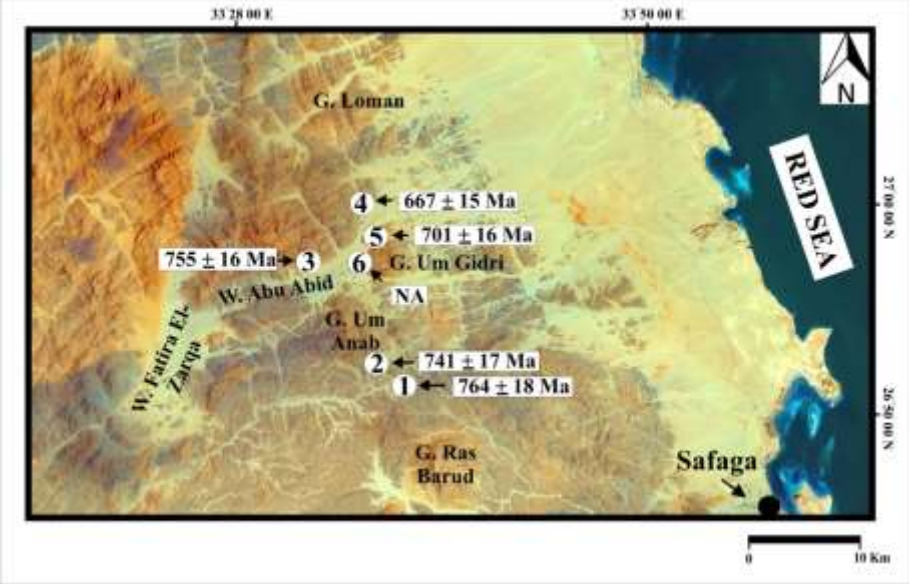

Fig. 2. Location map for analyzed samples along Wadi Abu Abid (the solid black line in Fig. 1), showing the zircon U-Pb Concordia age of the examined samples with 2σ error ranges. Sample number are 1,2,3,4,5, and 6 are the same sample presented in Table 1.

Table 1. The analyzed granitoid samples.

Sample	Location		Elev.	Th/U	Rock Type	Rock unites traditional classification	Concordant	
	Lat.	Long.					Age (Ma)	± 2σ (Ma)
	Syn-orogenic							
WAA2	26°51'50.06"N	33°36'10.21"E	879	0.454	Granodiorite	Older Granite	764	18
WAA3	26°57'25.04"N	33°32'29.95"E	648	0.701	Monzogranite	Younger Granite	755	16
WAA1	26°52'28.59"N	33°33'53.78"E	915	0.599	Monzogranite	Younger Granite	741	17
WAA5	26°58'20.45"N	33°34'43.52"E	566	0.435	Monzogranite	Younger Granite	701	16
WAA4	26°59'54.29"N	33°34'10.37"E	512	0.394	Alkali-feldspar granite	Younger Granite	667	15
WAA6	26°57'57.64"N	33°35'6.29"E	595	-	Monzogranite	Younger Granite	-	-

Elev.: Elevation in meters.
Lat.: Latitude in degrees, minutes, seconds.
Long.: longitude in degrees, minutes, seconds.

2. GEOLOGIC SETTING

Wadi Abu Abid area represents the NED basement rocks, which, in turn, falls in the northern part of the ANS (Fig. 1). Compared with CED and SED, the NED area basements are mainly noted by less deformation rare volcanic activities [13], and nearly no Banded Iron Formation (BIF) (e.g., [24], [25], [13]). The NED resembles the Sinai basements by abundant granitoid outcrops and rare volcanic exposures (e.g., [6], [7], [23]). Based on the ANS evolutionary events, the basement outcrops can be generally grouped as : (a) Pre-collision (ca. 820–750 Ma) rocks of mainly highly deformed to green schist facies, graded metavolcanics, metasediments, and granitoids with island arcs affinities (e.g., [11], [12], [26], [27], [28]). (b) Syn-collision (ca. 750–630 Ma) less deformed granitoids compared to the Pre-collisional type [16], [18], [19], [29]. (c) Post-collision (ca. 630–560 Ma) rocks represented mainly by extensional intraplate undeformed granitoids [30], [31], [32]. Dyke swarms mainly started during the last

phase of the post-collision stage (ca. 590-550 Ma) [26], marking the continuous extension regime after the termination of EAO [15].

Geochemically, Farahat et al., [4] studied two areas above and below the study area geochemically. The El Bula area exposures (in the south) were found to be dominated by calc-alkaline metaluminous to mildly peraluminous I-type tonalitic and granodioritic rocks. These granitoids are suggested to be of island-arc rocks of the pre-collision stage. They originated from either high-degree partial melting (~40%) of a mafic deep crustal source (amphibolitic batholith) or fractional crystallization evolution compared with the post-collision mantle-derived magmatism recorded in the NED (e.g., [22]). While the Loman area (in the north) is dominated by a mid-alkaline to metaluminous A-type alkali-granite suite of the post-orogenic phase. The source of this magma is recommended to be a partial melting of a tonalitic source in the middle crust followed by fractional crystallization during the post-collisional extensional stage.

Chronologically, Eliwa et al., [33] studied the Dara area (northeast of the study area) in the NED, where the granitoids represented by trondhjemite, granodiorite, biotite-hornblende granite, and alkali-feldspar granites with a U–Pb age (Ma) of 741 ± 2.9, 720 ± 7, 608 ± 2.9, and 600 ± 3, respectively. Mansour et al., [23] conclude the older granites ages of 758 ± 5 Ma reaches to 653 ± 7 Ma, which represented by both calc-alkaline and alkaline granitic rocks.

Tectonically, the area may be affected by post-crystallization different regional tectonic events, supported by the zircon and apatite fission-track data (Thermotectonic analysis) from the G. Loman area granites [34]; In the northern border of the study area, as three tectonic events are recorded (Hercynian tectonic activity, Gondwana disintegration, and the Red Sea/Suez rift System), the same events are recorded in several places in the Eastern Desert and Sinai ([35], [36], [37], [38], [39], [40], [41], [42], [43]). Trace minerals chemistry of zircon, far south of the study area, suggests several stages of granitic rocks formation as well [44].

The shortage in geochronological studies in the ANS, especially in the NED, induced a gap between the geochemical and geochronological studies of the rock units and created a difficulty in conducting a tectonic evolution model for the ANS. Therefore, we conduct this geochronological study using the zircon U-Pb technique on samples from the OG rocks in the Wadi Abu Abid area as a representative of the basement outcropping of the northern ANS in the NED. These were plotted on the IUGS quartz (Q)–alkali feldspar (A)–plagioclase (P) diagram for plutonic rocks, in which the samples were plotted on the corresponding fields based on the apparent QAP percentage in hand specimens (Fig. 3), four samples fall in the monzogranitic field, one in the alkali-feldspar granite zone, and the last one in the granodioritic area.

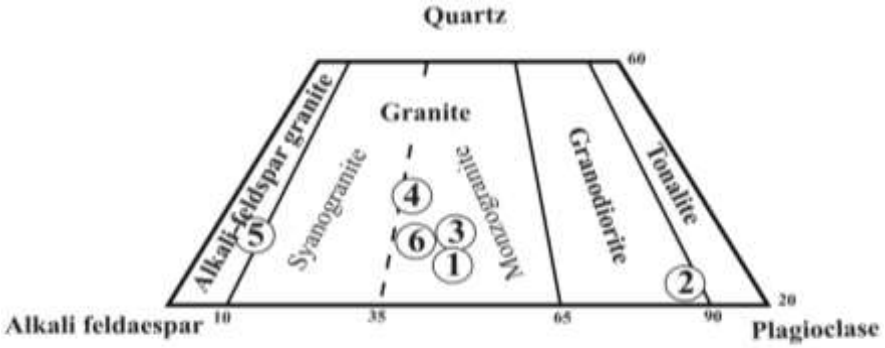

Fig. 3. IUGS quartz–alkali feldspar–plagioclase diagram in which the analyzed granitic samples plotted on.

These six granite samples can be traditionally categorized into two groups, Older and Younger granites, supported by many workers on the Egyptian granites (e.g., [6], [21], [45]).

2. METHODOLOGY

The collected granitic samples were prepared for the geochronological analysis through a set of steps: (1) The granitic samples (average weight 2-3 kg) were crushed using a geological hammer, and then a jaw crusher was used to reach a size ranging from 2 mm to mud size (< 0.063). (2) A sieving method was applied to remove the bigger and smaller size grains from the sand-sized grains. These steps were performed at the Geology Department, Port Said University, Port Said, Egypt. (3) Zircon crystals were separated using the heavy liquid separation methods [26], then through hand picking. (4) The U/Pb and Th/Pb isotopic ratios were measured using the LA-ICP-MS system at Kanazawa University, Japan. Table 2 gives brief information about specifications and operating conditions of the LA-ICP-MS setup that was applied in Tamura et al. [46]. .

Table 2. Specifications and operating conditions of the LA-ICP-MS.

ICP-MS	
Model	Agilent 7850
Forward power	1200 W
Plasma gas flow	15 L min^{-1}
Carrier gas flow	1.10 L min^{-1} (Ar), 0.3 L min^{-1} (He)
Interface	Ni sampler/Ni skimmer
Laser	
Model	UP-213 (New Wave Research)
Wavelength	213 nm (Nd-YAG)
Spot size	25 µm
Repetition rate	5 Hz
Energy density	7 J cm^{-2} (Attenuater: 50%–60%)
Warming up	10 sec

To ensure the validity of our measurements, zircon references with verified ages were frequently examined. Our measurements for the Zircon references ages are 28.8 ± 0.3, 612 ± 2, 1099 ± 2, 341 ± 2 Ma for Fish Canyon tuff, GJ-1, AS-3, and Plěsovice, respectively. These show an agreement with the previously reported reference ages of 28.4, 609, 1099, and 337.1 Ma [47], [48], [49], [50].

Throughout the analytical procedures, LA-ICP-MS signals; which used many works (e.g., [23], [26], [29], [32], [37], [51])were continuously inspected to ensure their stability and consistency and free from inclusions, core–rim compositional variation, zones commonly enriched in Pb, or evidence of signal fractionation. Following background correction, mean isotopic intensities were calculated to derive the isotopic ratios [52]. The 204Pb (and 204Hg) were repeatedly below the detection limit as shown in Table 3, therfore, the reported ages are not corrected for 204Pb. The reported concordant ages, along with their 2σ uncertainties that are presented in the text and figures, are calculated using the IsoplotR [53], as it used in many researches for the same purpose (e.g., [23], [29], [32], [37]).

Gr.	Intensities and 3σ D. L.		Conce. (µg/g) and 2σ Errors		Isotopic Ratios and 2σ Errors						Age (Ma) and 2σ Errors						%Discord.		
	^{204}Pb	^{238}U	Th/U	2σ	$^{206}Pb/^{238}U$	2σ	$^{207}Pb/^{235}U$	2σ	$^{208}Pb/^{232}Th$	2σ	$^{206}Pb/^{238}U$	2σ	$^{207}Pb/^{235}U$	2σ	$^{207}Pb/^{206}Pb$	2σ	Conc.	2σ	
WAA01																			
*D7	0.0073	430.6	0.43	0.043	0.08106	0.00811	0.67447	0.06745	0.02935	0.00294	502	47	523	40	616	194	517	39	4.0
*D9	0.0255	70.9	0.35	0.034	0.19289	0.01929	2.38371	0.23837	0.08634	0.00863	1137	102	1238	70	1418	163	1228	73	8.1
*E1	0.0487	95.0	0.26	0.025	0.20490	0.02049	2.34826	0.23483	0.06545	0.00655	1202	107	1227	70	1272	160	1227	70	2.0
F5	0.0551	317.9	0.33	0.033	0.11683	0.01168	1.09721	0.10972	0.04062	0.00406	712	66	752	52	872	146	748	53	5.3
F7	0.0177	109.5	0.70	0.070	0.13016	0.01302	1.11069	0.11107	0.03887	0.00389	789	73	759	52	670	148	757	52	-3.9
H8	0.0097	111.9	0.72	0.071	0.11815	0.01181	1.13917	0.11392	0.04004	0.00400	720	67	772	53	926	137	769	55	6.7
H10	2.3086	3.6	1.44	0.143	0.11693	0.01169	1.08879	0.10888	0.03620	0.00362	713	66	748	52	854	152	744	53	4.6
I2	0.6089	210.8	0.47	0.047	0.12007	0.01201	1.15538	0.11554	0.04008	0.00401	731	68	780	53	922	124	782	55	6.2
*I3	10.397	855.7	1.18	0.118	0.31639	0.03164	5.34542	0.53454	0.10283	0.01028	1772	152	1876	84	1993	144	1887	84	5.5
I5	0.2944	151.0	0.29	0.029	0.12552	0.01255	1.17504	0.11750	0.04088	0.00409	762	70	789	54	865	111	795	54	3.4
J10	0.6392	455.7	0.42	0.041	0.12380	0.01238	1.14814	0.11481	0.04462	0.00446	752	70	776	53	846	138	776	54	3.0
WAA02																			
F2	0.0426	554.7	0.15	0.015	0.13490	0.013	1.24371	0.12437	0.04323	0.00432	816	75	821	55	834	132	821	55	0.6
F4	0.0296	332.3	0.24	0.024	0.13050	0.013	1.17919	0.11792	0.04242	0.00424	791	73	791	54	792	242	791	49	0.0
G1	0.7548	174.5	0.06	0.005	0.13979	0.013	1.36760	0.13676	0.04687	0.00469	843	77	875	57	956	184	869	57	3.7
*G7	0.1083	529.5	0.07	0.006	0.35110	0.035	6.16722	0.61672	0.10799	0.01080	1940	164	2000	86	2062	145	2006	85	3.0
H4	0.0187	73.4	0.88	0.088	0.12257	0.012	1.21767	0.12177	0.04457	0.00446	745	69	809	55	987	98	829	56	7.9
H9	0.0022	88.6	0.96	0.096	0.10867	0.01087	0.87928	0.08793	0.03380	0.00338	665	62	641	47	555	228	647	43	-3.7
H10	0.6241	1503.1	0.70	0.069	0.11571	0.01157	0.99917	0.09992	0.03847	0.00385	706	66	703	50	696	175	704	49	-0.4
I7	0.7700	1070.1	0.57	0.057	0.12346	0.01235	1.10503	0.11050	0.03956	0.00396	750	69	756	52	772	160	755	52	0.8
I9	0.0221	96.5	0.37	0.036	0.12629	0.01263	1.13418	0.11342	0.03951	0.00395	767	71	770	53	779	146	770	53	0.4
I10	0.0054	176.8	0.05	0.005	0.12597	0.01260	1.19045	0.11905	0.04204	0.00420	765	71	796	54	885	137	796	55	3.9
*J2	1.7544	117.6	0.95	0.095	0.25455	0.02546	3.72190	0.37219	0.08360	0.00836	1462	128	1576	78	1733	108	1616	73	7.2
WAA03																			
B1	0.1271	116.9	0.49	0.04923	0.11560	0.01156	1.04765	0.10477	0.03855	0.00386	705	65	728	51	798	133	728	52	3.2
B10	-0.0005	79.7	0.79	0.078755	0.11790	0.01179	1.06317	0.10632	0.03972	0.00397	718	67	735	51	787	242	730	46	2.3
D4	0.0687	115.1	0.57	0.056678	0.12709	0.01271	1.16266	0.11627	0.03971	0.00397	771	71	783	53	817	188	781	53	1.5
F5	0.0638	196.3	0.48	0.04842	0.12460	0.01246	1.11766	0.11177	0.03943	0.00394	757	70	762	53	776	172	761	52	0.7
G8	0.0722	133.6	0.34	0.03416	0.10758	0.01076	0.95371	0.09537	0.03497	0.00350	659	61	680	49	751	101	687	49	3.1
G10	0.0152	98.0	0.04	0.00430	0.12533	0.01253	1.07154	0.10715	0.03972	0.00397	761	70	739	51	674	142	738	51	-2.9
I1	-0.0036	57.8	0.51	0.051044	0.12560	0.01256	1.16899	0.11690	0.04032	0.00403	763	70	786	54	853	132	787	54	2.9
I4	0.0057	65.0	0.56	0.055596	0.13431	0.01343	1.28988	0.12899	0.04477	0.00448	812	75	841	56	918	128	844	57	3.4

Gr.	Intensities and 3σ D. L.		Conce. (µg/g) and 2σ Errors		Isotopic Ratios and 2σ Errors						Age (Ma) and 2σ Errors								%Disc ord.
	^{204}Pb	^{238}U	Th/ U	2σ	$^{206}Pb/^{238}U$	2σ	$^{207}Pb/^{235}U$	2σ	$^{208}Pb/^{232}Th$	2σ	$^{206}Pb/^{238}U$	1σ	$^{207}Pb/^{235}U$	1σ	$^{207}Pb/^{206}Pb$	1σ	Conc.	σ	
I5	0.0052	16.4	2.26	0.22595	0.12500	0.01250	1.08873	0.10887	0.04067	0.00407	759	70	748	52	714	125	746	51	-1.4
J4	0.738	263.9	0.75	0.07473	0.11853	0.01185	1.10525	0.11052	0.03987	0.00399	722	67	756	52	857	138	755	53	4.5
J7	0.130	217.8	0.92	0.09165	0.13271	0.01327	1.25566	0.12557	0.04476	0.00448	803	74	826	55	887	111	832	55	2.8
WAA04																			
D1	0.0049	35.8	0.22	0.02186	0.10819	0.01082	0.96726	0.09673	0.03588	0.00359	662	62	687	49	769	134	687	50	3.6
E2	-0.0033	126.6	0.36	0.03635	0.11082	0.01108	0.91663	0.09166	0.03534	0.00353	678	63	661	48	603	249	666	43	-2.5
E10	-0.0058	110.4	0.28	0.02810	0.10773	0.01077	0.92859	0.09286	0.03414	0.00341	660	61	667	48	692	192	665	47	1.0
F8	0.0039	204.8	0.21	0.02097	0.10659	0.01066	0.84411	0.08441	0.03320	0.00332	653	61	621	46	508	180	625	45	-5.1
H2	0.0512	401.8	0.21	0.02089	0.11467	0.01147	0.95412	0.09541	0.03471	0.00347	700	65	680	49	616	104	672	46	-2.9
H3	-0.0067	195.4	0.29	0.02871	0.11385	0.01138	0.98961	0.09896	0.03604	0.00360	695	65	699	49	710	141	699	50	0.6
H9	-0.0117	184.5	0.38	0.03755	0.11046	0.01105	0.98918	0.09892	0.03540	0.00354	675	63	698	49	773	134	698	50	3.3
J2	-0.0083	590.9	0.05	0.00524	0.10741	0.01074	0.92879	0.09288	0.03389	0.00339	658	61	667	48	699	132	667	48	1.3
J7	4.0088	374.7	1.02	0.10230	0.11234	0.01123	0.96883	0.09688	0.03546	0.00355	686	64	688	49	693	125	688	49	0.3
J9	0.3995	30.6	0.92	0.09205	0.10694	0.01069	0.86650	0.08665	0.03449	0.00345	655	61	634	46	558	145	633	46	-3.3
WAA05																			
A4	-0.0089	117.4	0.54	0.05365	0.10609	0.01061	0.93168	0.09317	0.03415	0.00341	650	61	669	48	731	134	668	49	2.8
A5	0.0051	75.4	0.39	0.03891	0.12141	0.01214	1.08187	0.10819	0.03807	0.00381	739	68	745	52	762	243	743	47	0.8
F1	-0.0072	35.8	0.31	0.03141	0.10882	0.01088	0.88586	0.08859	0.03515	0.00351	666	62	644	47	569	195	648	45	-3.4
G5	0.0075	131.1	0.50	0.05045	0.11006	0.01101	0.92691	0.09269	0.03414	0.00341	673	63	666	48	642	176	667	47	-1.0
G8	-0.0069	61.7	0.31	0.03149	0.11847	0.01185	1.06005	0.10600	0.03763	0.00376	722	67	734	51	771	101	738	50	1.6
H1	-0.0018	58.5	0.20	0.01965	0.11203	0.01120	0.93409	0.09341	0.03376	0.00338	685	64	670	48	620	143	669	48	-2.2
H3	0.0118	95.0	0.43	0.04286	0.11166	0.01117	0.99578	0.09958	0.03719	0.00372	682	63	702	50	764	134	702	50	2.8
H8	-0.0101	76.1	0.50	0.04976	0.11596	0.01160	1.06306	0.10631	0.03922	0.00392	707	66	735	51	822	129	736	52	3.8
J4	-0.0052	105.5	0.58	0.05806	0.12400	0.01240	1.08701	0.10870	0.03866	0.00387	754	70	747	52	728	125	746	51	-0.9
J9	0.0016	112.6	0.58	0.05847	0.11679	0.01168	1.07759	0.10776	0.03795	0.00380	712	66	742	52	835	138	742	53	4.0

3. RESULTS

Zircon U-Pb data were acquired from 53 grains separated from 5 granitic samples (sample WAA6 gives no results). Grains with detectable levels of common lead, cracks, or inclusions were removed from sample age calculations and discussions. Grains with concordance less than 90%, cracks, or inclusions were removed from the calculation processes, giving the concordant $^{206}Pb/^{238}U$ age of the grains in each of the studied sample, so that from a total of 53 zircon U-Pb data sample 47 grains give more age credibility to achieve a more accurate crystallization ages.

For WAA1 sample (Fig. 2), 11 zircon grains were analyzed (Table 3), showing different transparency degrees from yellow to brown colors. They are mainly euhedral crystals, with a length/width average ratio of 2:1. Most of them had minor inclusions, with nearly 65% of them showing prominent cracks. The isotopic ratios Th/U range from 0.29 to 1.44, with 0.62 as an average value. D7 grain were removed from the age determination as it gives a younger age of 517 ± 39 Ma (Table 3), and in contrast grains D9, E1, and I3 give older pre-Pan-African ages of 1228 ± 73 Ma, 1227 ± 73 Ma, and 1887 ± 80 Ma in respect, so they were also removed from the age determination. The 7 remaining grains display a single age cluster, giving an age of 741 ± 17 Ma (Fig. 4), which represents the age of crystallization of the studied monzogranite rock sample (Table 1; Fig. 4).

For WAA2 sample (Fig. 2), a total of 11 grains were analyzed (Table 3), with a transparent to yellow color and mainly euhedral crystal faces, with a length/width average ratio of approximately 3:1. The majority of grains have small inclusions, with nearly 70% of them show prominent cracks. Th/U ratios range between 0.06 to 0.96, with 0.44 as an average value. Grains G7 and J2 give discordant older ages of 2006 ± 56 and 1616 ± 73, respectively, so they were removed from the sample age determination. The 9 remaining grains display a mean age forming a single aggregate, giving an age of 764 ± 18 Ma (Fig. 4), which indicates the age of crystallization of the studied granodiorite rock sample (Fig. 4; Table 1).

For WAA3 sample (Fig. 2), 11 zircon grains were analyzed (Table 3), showing different transparency degrees from yellow to brown colors. They are mainly euhedral crystals, with a length/width average ratio of 2:1. Most of them had inclusions, and nearly 65% of them show prominent cracks. The Th/U ratios vary between 0.04 and 2.26, giving an average value of 0.7. All 11 grains show a uniform clustering on the Concordia, providing a concordant age of 755 ± 16 Ma (Fig. 4), the 755 ± 16 Ma age reflecting the formation age of the analyzed monzogranite sample (Table 1; Fig. 4).

For WAA4 sample (Fig. 2), a total of 10 grains were analyzed (Table 3), showing a range of transparency variation from transparent with frequent yellow discoloration. Most zircons are primary euhedral crystals, with a 3:1 is the average length/width ratio. The majority of grains contain small inclusions, and approximately 60% of them show prominent cracks. The isotopic ratios Th/U range from 0.05 to 1.02, with 0.39 as an average value. All analyzed zircon grains show a uniform aggregation giving

a Concordia age of 667 ± 15 Ma (Fig. 4), which is interpreted as the formation age of the alkali-feldspar granite (Table 1; Fig. 4). the same age shown as a reworked zircon grain age in the Fawakhir alkali-feldspar granite sample with a Concordia age 564.3 ± 7.8 Ma south of the current study area [29].

For WAA5 sample (Fig. 2), 10 zircon grains were analyzed (Table 3), showing different transparency degrees from yellow to brown colors. Crystals are mainly euhedral, with a length/width average ratio of 2:1. Most of the zircons had inclusions, with nearly 65% of them showing prominent cracks. The Th/U ratios vary between 0.31 to 0.58, giving an average value of 0.43. All analyzed zircon grains allocated in a single age population, giving a mean age of 701 ± 16 (Fig. 4), which represents the age of the monzogranite studied rock sample crystallization age (Table 1; Fig. 4).

Table 4. Summary of Wadi Abu Abid samples Concordia age with Mean Square of Weighted Deviation (MSWD), and number of zircon grains (n).

Num.	Code	Zircon age	MSWD	n
1	WAA01	741 ± 17 Ma	54	11
2	WAA02	764 ± 18 Ma	3.5	11
3	WAA03	755 ± 16 Ma	3	11
4	WAA04	667 ± 15 Ma	1.1	10
5	WAA05	701 ± 16 Ma	2.5	10

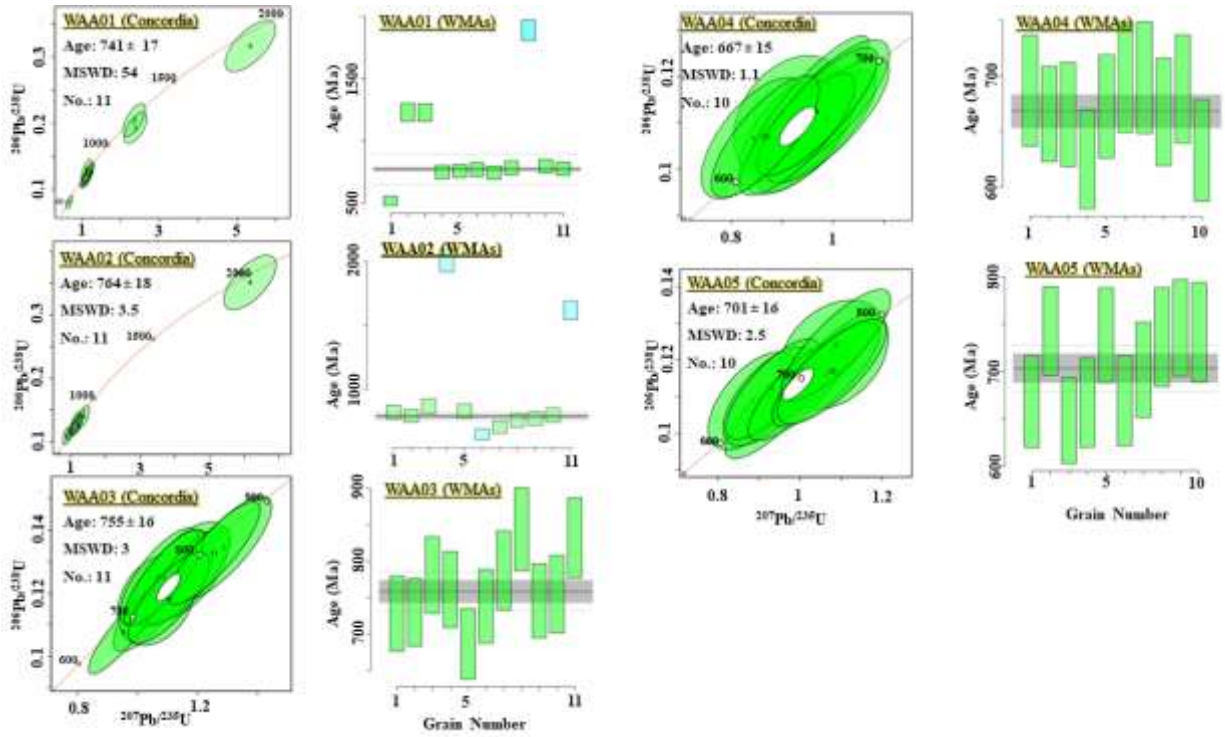

Fig. 4. Concordia diagrams and weighted mean ages distributions for all zircon grains, plotted using IsopltR [53].

5. DISCUSSION

The majority of the analyzed zircons give an average Th/U isotopic value ranging from 0.05 to 2.26, showing an average value of 0.51 (Table 3). On the basis of the various analyses of magmatic and metamorphic zircons [54], [55]. That wide ratio reflects a magmatic source for the zircon crystal, with the exception of five zircon grains. These grains show a lower Th/U isotopic value than 0.1.

WAA2, WAA3, WAA1, WAA5, and WAA4 samples show a U-Pb Concordia age of 764 ± 18 Ma, 755 ± 16 Ma, 741 ± 17 Ma, 701 ± 16 Ma, and 667 ± 15 Ma, respectively (Table 1; Fig. 2) (Cryogenian Period), which are all located within the Syn-collisional magmatic [16], [18], [19], [29].

Xenocrysts with pre-EAO ages have been yielded by our samples; grains D9, E1, and I3 in sample WAA1; and grains G7 and J2 in sample WAA2 yielded ages of 1228 ± 73 Ma, 1227 ± 70 Ma, 1887 ± 84 Ma, 2006 ± 85 Ma, and 1616 ± 73 Ma, respectively (Fig. 5; Table 3). These ages indicate a probable Pre-Neoproterozoic material engagement that infected the magma generation or emplacement, reflecting inheritance from older crustal basement (e.g., [26], [56], [57]). The presence of these pre-EAO grains raises a question about the possibility of the former existence of pre-Pan-African crust, which needs a more detailed and vast investigation along the rock units forming the ANS crust as noted in other similar approaches in the Eastern Desert (e.g., [32], [29],[23], [51]).

A zircon grain gave a younger age that is not compatible with the sample's population age (517 ± 39 Ma, D7 grain in sample WAA1) (Fig. 5). This age either indicates a new growth during magmatic differentiation or overgrowth during metamorphism, and taking in consider the Th/U ratio (0.43), which indicates a magmatic source that is supported by its separated from a granitic sample (Table 1). This younger grain might indicate a further extension of post-collisional magmatic activity [26]. An alternative possibility is being an effect of the later dyke intrusion that affected the ANS [26].

The recorded Concordia ages of Syn-orogenic granitic show a general increase moving from SED to the study area in the NED, as diorite (OG) and syenite (YG) in Marsa Alam-Idfu transect (699.1 ± 4.3 Ma - 645.9 ± 1.7 Ma) [32], Older granite (729 ± 10 Ma) clastic part of Hammamat group along the Qift-Quseir transect [29], the granite (YG) and diorite (OG) of Safaga –Qena transect (758 ± 5 Ma - 653 ± 7 Ma) [23]. This increase of the Syn-orogenic granite recorded Concordia ages is continuing moving north of the study area (NED), as Mus trondhjemite and granodiorite (OG) of G. Dara area (741 ± 2.9 Ma & 720 ± 7 Ma) [33]. All of the previously mentioned Concordia ages used the LA-ICP-MS method, except for G. Dara area used SIMS (Secondary Ion Mass Spectrometer) zircon U–Pb dating.

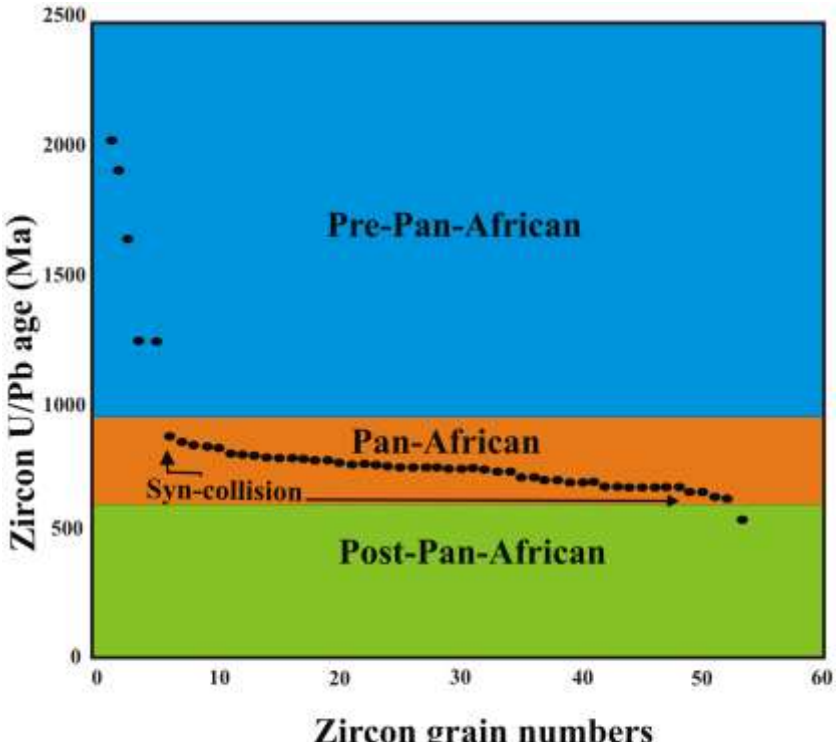

Fig. 5. Distribution chart shows the analyzed single zircon U-Pb concordant ages from all grains.

5. CONCLUSION

1. The NED basement outcrops at the studied region show one distinct magmatic event, the syn-collisional phase, characterized by the coexistence of "Gray, Older" calc-alkaline and "Red, Younger" alkaline granitic suites, positioned between 764 ± 18 Ma and 667 ± 15 Ma.
2. The traditional way of "Older" and "Younger" granitoids classification according to their apparent mineralogical composition and color variations gives misleading interpretations on the magmatic and tectonic sequences.
3. The presence of xenocryst zircon grains (2006 ± 85 Ma to 1227 ± 70 Ma) in the analyzed grains raises questions about the potential presence of craton basement composition, although rocks with pre-Neoproterozoic ages were absent in the study area.
4. The presence of zircon grain with an age of 517 ± 39 Ma indicates a possible continuity of the post-collisional activity in the ANS till this time.

Author Contributions: Conceptualization, S.M. and M. A. G.; methodology, S.M., M. A. G., M. O., and M. Z. E.; validation, S.M., M. A. G., M. O., and M. Z. E.; formal analysis, S.M., M. A. G., M. O., and M. Z. E.; investigation, S.M., M. A. G., M. O., and M. Z. E.; data curation, S.M., M. A. G., M. O., and M. Z. E.; writing—original draft preparation, M. A. G.; writing—review and editing, S.M., M. O., and M. Z. E.; visualization, S.M., M. A. G., M. O., and M. Z. E.; supervision, M. Z. E.; project administration, M. Z. E, S.M., M. O., and M. A. G.; All authors have read and agreed to the published version of the manuscript.

Data Availability Statement: The raw data supporting the conclusions of this article will be made available by the authors without undue reservation.

Conflicts of Interest: The authors declare no conflicts of interest.

6. REFERENCES

[1] S. El Gaby, F. K. List, and R. Tehrani, "The basement complex of the Eastern Desert and Sinai," in *The Geology of Egypt*, 1st Edition., 1990, pp. 175–184.

[2] M. Hassan and A. Hashad, "Precambrian of Egypt," in *The Geology of Egypt*, 1st ed., 1990, pp. 201–245.

[3] A. M. Moghazi, M. A. Hassanen, F. H. Mohamed, and S. Ali, "Late Neoproterozoic strongly peraluminous leucogranites, South Eastern Desert, Egypt ? petrogenesis and geodynamic significance," *Mineral. Petrol.*, vol. 81, no. 1–2, pp. 19–41, May 2004.

[4] E. S. Farahat, H. A. Mohamed, A. F. Ahmed, and M. M. El Mahallawi, "Origin of I- and A-type granitoids from the Eastern Desert of Egypt: Implications for crustal growth in the northern Arabian–Nubian Shield," *J. Afr. Earth Sci.*, vol. 49, no. 1–2, pp. 43–58, Sep. 2007.

[5] E. S. Farahat, R. Zaki, C. Hauzenberger, and M. Sami, "Neoproterozoic calc-alkaline peraluminous granitoids of the Deleihimmi pluton, Central Eastern Desert, Egypt: implications for transition from late- to post-collisional tectonomagmatic evolution in the northern Arabian–Nubian Shield," 2011.

[6] M. Z. El-Bialy and M. M. Omar, "Spatial association of Neoproterozoic continental arc I-type and post-collision A-type granitoids in the Arabian–Nubian Shield: The Wadi Al-Baroud Older and Younger Granites, North Eastern Desert, Egypt," *J. Afr. Earth Sci.*, vol. 103, pp. 1–29, 2015.

[7] M. Z. El-Bialy, "Precambrian Basement Complex of Egypt," in *The Geology of Egypt*, Z. Hamimi, A. El-Barkooky, J. Martínez Frías, H. Fritz, and Y. Abd El-Rahman, Eds., in Regional Geology Reviews. , Cham: Springer International Publishing, 2020, pp. 37–79.

[8] R. J. Stern, "ARC ASSEMBLY AND CONTINENTAL COLLISION IN THE NEOPROTEROZOIC EAST AFRICAN OROGEN: Implications for the Consolidation of Gondwanaland," *Annu. Rev. Earth Planet. Sci.*, vol. 22, no. 1, pp. 319–351, May 1994.

[9] R. J. Stern, "Crustal evolution in the East African Orogen: a neodymium isotopic perspective," *J. Afr. Earth Sci.*, vol. 34, no. 3–4, pp. 109–117, Apr. 2002, doi: 10.1016/S0899-5362(02)00012-X.

[10] P. R. Johnson *et al.*, "Late Cryogenian–Ediacaran history of the Arabian–Nubian Shield: A review of depositional, plutonic, structural, and tectonic events in the closing stages of the northern East African Orogen," *J. Afr. Earth Sci.*, vol. 61, no. 3, pp. 167–232, Oct. 2011.

[11] Y. K. Bentor, "THE CRUSTAL EVOLUTION OF THE ARABO--NUBIAN MASSIF WITH SPECIAL REFERENCE TO THE SINAI PENINSULA," *Precambrian Res.*, vol. 28, no. 1, pp. 1–74, 1985.

[12] A. Kröner, "Age and tectonic setting of granitoid gneisses in the Eastern Desert of Egypt and south-west Sinai," *Springer Int. Publ.*, vol. 83, pp. 502–513, 1994.

[13] M. Z. El-Bialy *et al.*, "U-Pb zircon geochronology and geochemical constraints on the Ediacaran continental arc and post-collision Granites of Wadi Hawashiya, North Eastern Desert, Egypt:

Insights into the ~600 Ma crust-forming Event in the northernmost part of Arabian-Nubian Shield," *Precambrian Res.*, vol. 345, p. 105777, Aug. 2020, doi: 10.1016/j.precamres.2020.105777.

[14] J. G. Meert, "A synopsis of events related to the assembly of eastern Gondwana," *Tectonophysics*, vol. 362, no. 1–4, pp. 1–40, Feb. 2003, doi: 10.1016/S0040-1951(02)00629-7.

[15] H. Fritz *et al.*, "Orogen styles in the East African Orogen: A review of the Neoproterozoic to Cambrian tectonic evolution," *J. Afr. Earth Sci.*, vol. 86, pp. 65–106, Oct. 2013, doi: 10.1016/j.jafrearsci.2013.06.004.

[16] R. J. Stern and C. E. Hedge, "Geochronologic and isotopic constraints on late Precambrian crustal evolution in the Eastern Desert of Egypt.," *Am. J. Sci.*, vol. 285 (2), pp. 97–127, 1985.

[17] M. Eyal, B. Litvinovsky, B. M. Jahn, A. Zanvilevich, and Y. Katzir, "Origin and evolution of post-collisional magmatism: Coeval Neoproterozoic calc-alkaline and alkaline suites of the Sinai Peninsula," *Chem. Geol.*, vol. 269, no. 3–4, pp. 153–179, Jan. 2010, doi: 10.1016/j.chemgeo.2009.09.010.

[18] A.-K. M. Moghazi, "Magma source and evolution of Late Neoproterozoic granitoids in the Gabal El-Urf area, Eastern Desert, Egypt: geochemical and Sr–Nd isotopic constraints," *Geol. Mag.*, vol. 136, no. 3, pp. 285–300, May 1999, doi: 10.1017/S0016756899002563.

[19] A. M. Moghazi, "Petrology and geochemistry of Pan-African granitoids, Kab Amiri area, Egypt - implications for tectonomagmatic stages in the Nubian Shield evolution," *Mineral. Petrol.*, vol. 75, no. 1–2, pp. 41–67, May 2002, doi: 10.1007/s007100200014.

[20] A. G. Waheeb, "RESOLVED SHEAR FOR THE URANIUM MINERALIZED FAULT CONTACTS AT GABAL ABU HAMR AND GABAL GATTAR, NORTHERN EASTERN DESERT, EGYPT," *Ann. Geol Surv Egypt*, pp. 243–255, 2021.

[21] K. M. Abdelfadil *et al.*, "Composite Granitic Plutonism in the Southern Part of the Wadi Hodein Shear Zone, South Eastern Desert, Egypt: Implications for Neoproterozoic Dioritic and Highly Evolved Magma Mingling during Volcanic Arc Assembly," *Minerals*, vol. 14, no. 10, p. 1002, Oct. 2024, doi: 10.3390/min14101002.

[22] K. M. Abdelfadil *et al.*, "Post-Collisional Mantle Processes and Magma Evolution of the El Bola Mafic–Ultramafic Intrusion, Arabian-Nubian Shield, Egypt," *Minerals*, vol. 15, no. 7, p. 705, Jul. 2025, doi: 10.3390/min15070705.

[23] S. Mansour, A. M. Abu-Elsaoud, F. Haouala, M. Z. Khedr, A. Tamura, and N. Hasebe, "Geochronological Evolution of the Safaga–Qena Transect, Northern Eastern Desert, Egypt: Implications of Zircon U-Pb Dating," *Minerals*, vol. 15, no. 5, p. 532, May 2025, doi: 10.3390/min15050532.

[24] G. H. E. Habaak, "PETROGENESIS AND TECTONIC IMPLICATIONS OF THE ROCK SUCCESSION HOSTING BANDED IRON FORMATION AT UM ANAB AREA, NORTH EASTERN DESERT OF EGYPT," *FOURTH Int. Conf. Geol. Afr.*, vol. 2, pp. 479–513, 2005.

[25] F. F. Basta, A. E. Maurice, L. Fontboté, and P.-Y. Favarger, "Petrology and geochemistry of the banded iron formation (BIF) of Wadi Karim and Um Anab, Eastern Desert, Egypt: Implications for the origin of Neoproterozoic BIF," *Precambrian Res.*, vol. 187, no. 3–4, pp. 277–292, Jun. 2011, doi: 10.1016/j.precamres.2011.03.011.

[26] S. Mansour, N. Hasebe, J. G. Meert, A. Tamura, F. I. Khalaf, and M. K. El-Shafei, "Evolution of the Arabian-Nubian Shield in Gabal Samra area, Sinai; implications from zircon U–Pb geochronology," *J. Afr. Earth Sci.*, vol. 192, p. 104538, Aug. 2022.

[27] R. O. Greiling, M. M. Abdeen, and A. A. Dardir, "A structural synthesis of the Proterozoic Arabian-Nubian Shield in Egypt," vol. 83, pp. 484–501, 1994.

[28] K. El-Gameel, S. Fayed, H. El Desouky, and A. Abdelmaksoud, "Geological studies and structural analysis of the Umm Anab metavolcanics and related quartz veins: implications for Pan-African volcanism in the Egyptian Nubian Shield," *Egypt. J. Geol.*, vol. 67, no. 1, pp. 243–259, Dec. 2023.

[29] S. Mansour *et al.*, "Geochronological assessment of the Arabian-Nubian Shield plutonic intrusions in the arc assemblages along the Qift-Quseir transect, Central Eastern Desert of Egypt," *J. Afr. Earth Sci.*, vol. 220, p. 105456, Dec. 2024, doi: 10.1016/j.jafrearsci.2024.105456.

[30] A. A. A. Hussein, M. M. Ali, and M. F. El Ramly, "A proposed new classification of the granites of egypt," *J. Volcanol. Geotherm. Res.*, vol. 14, no. 1–2, pp. 187–198, Oct. 1982.

[31] A. M. H. Asran, M. A. Hassan, B. H. Ali, and A. I. Embaby, "GEOLOGICAL AND GEOCHEMICAL INVESTIGATIONS OF THE PAN-AFRICAN ROCKS ALONG WADI EL-ATRASH AREA, NORTH EASTERN DESERT, EGYPT.," pp. 89–113, 2008.

[32] S. Mansour *et al.*, "Development of the Arabian-Nubian Shield along the Marsa Alam-Idfu transect, Central-Eastern Desert, Egypt: geochemical implementation of zircon U-Pb geochronology," *Geochem. Trans.*, vol. 25, no. 1, p. 11, Oct. 2024, doi: 10.1186/s12932-024-00095-7.

[33] H. A. Eliwa *et al.*, "SIMS zircon U–Pb and mica K–Ar geochronology, and Sr–Nd isotope geochemistry of Neoproterozoic granitoids and their bearing on the evolution of the north Eastern Desert, Egypt," *Gondwana Res.*, vol. 25, no. 4, pp. 1570–1598, May 2014.

[34] S. Mansour, M. A. Gharib, N. Hasebe, K. Abdelrahman, M. S. Fnais, and A. Tamura, "Tectonic evolution of the Gabal Loman area, North Eastern Desert, Egypt: implications from low-temperature multithermochronometry on the Arabian-Nubian shield," *Front. Earth Sci.*, vol. 11, Jul. 2023, doi: 10.3389/feart.2023.1193692.

[35] S. Mansour, N. Hasebe, M. Z. Khedr, A. Tamura, and A. A. Shehata, "Tectonic-Thermal Evolution of the Wadi El-Dahal Area, North Eastern Desert, Egypt: Constraints on the Suez Rift Development," *Minerals*, vol. 13, no. 8, p. 1021, Jul. 2023, doi: 10.3390/min13081021.

[36] S. Mansour, N. Hasebe, U. A. Glasmacher, A. Tamura, and M. K. El-Shafei, "New insights into the thermo-tectonic development of the Suez rift within the framework of the northern Arabian–Nubian Shield," *Earth Surf. Process. Landf.*, vol. 50, no. 1, Jan. 2025, doi: 10.1002/esp.6054.

[37] S. Mansour, N. Hasebe, E. Azab, A. Y. Elnaggar, and A. Tamura, "Combined Zircon/Apatite U-Pb and Fission-Track Dating by LA-ICP-MS and Its Geological Applications: An Example from the Egyptian Younger Granites," *Minerals*, vol. 11, no. 12, p. 1341, Nov. 2021.

[38] S. Mansour, "Tectonic Development of Wadi Mi'ar Area, Sinai, Egypt: Implications of Low-Temperature Thermochronology Techniques," *Alfarama J. Basic Appl. Sci.*, vol. 0, no. 0, pp. 0–0, Jul. 2023, doi: 10.21608/ajbas.2023.218033.1160.

[39] S. Mansour, N. Hasebe, K. Abdelrahman, M. S. Fnais, and A. Tamura, "Reconstructing the Tectonic History of the Arabian–Nubian Shield in Sinai: Low-Temperature Thermochronology Implications on Wadi Agar Area," *Minerals*, vol. 13, no. 4, p. 574, Apr. 2023.

[40] S. Mansour *et al.*, "Thermochronological Constraints on the Tectonic History of the Arabian–Nubian Shield's Northern Tip, Sinai, Egypt," *Minerals*, vol. 14, no. 12, p. 1246, Dec. 2024, doi: 10.3390/min14121246.

[41] S. Mansour, N. Hasebe, K. Abdelrahman, M. S. Fnais, and A. Tamura, "The Gulf of Suez rifting: implications from low-temperature thermochronology," *Int. Geol. Rev.*, vol. 67, no. 5, pp. 694–710, Nov. 2024.

[42] S. Mansour and M. A. Gharib, "Tectonic Assessment of the Northwestern Nubian Shield at Southern Sinai, Egypt," *Spectr. Sci. J.*, vol. 2, no. 1, pp. 17–31, Apr. 2025.

[43] S. Mansour, A. Elkelish, A. S. Alawam, M. A. Gharib, A. Tamura, and N. Hasebe, "Tectonic Evolution of Wadi Hebran Area on the Suez Rift Eastern Flank, Sinai, Egypt," *Minerals*, vol. 15, no. 6, p. 655, Jun. 2025, doi: 10.3390/min15060655.

[44] K. M. Abdelfadil, M. E. Gharib, P. Uher, and M. Putiš, "Petrogenesis of post-orogenic Pan-African rare-element granitic pegmatites in the western Arabian-Nubian Shield, Aswan area, southern Egypt," *J. Asian Earth Sci.*, vol. 224, p. 105003, Feb. 2022, doi: 10.1016/j.jseaes.2021.105003.

[45] M. M. Mogahed and K. M. Abdelfadil, "Constraints of Mantle and Crustal Sources Interaction during Orogenesis of Pre- and Post-collision Granitoids from the Northern Arabian-Nubian Shield: A Case Study from Wadi El-Akhder Granitoids, Southern Sinai, Egypt," *Acta Geol. Sin. - Engl. Ed.*, vol. 95, no. 5, pp. 1527–1550, Oct. 2021, doi: 10.1111/1755-6724.14769.

[46] A. Tamura, T. Sagawa, K. Okino, and T. Morishita, "Determination of whole-rock trace-element compositions of siliceous rocks using MgO-diluted fused glass and LA–ICP–MS," *Geochem. J.*, vol. 56, no. 6, pp. 231–239, 2022, doi: 10.2343/geochemj.GJ22020.

[47] S. E. Jackson, N. J. Pearson, W. L. Griffin, and E. A. Belousova, "The application of laser ablation-inductively coupled plasma-mass spectrometry to in situ U–Pb zircon geochronology," *Chem. Geol.*, vol. 211, no. 1–2, pp. 47–69, Nov. 2004, doi: 10.1016/j.chemgeo.2004.06.017.

[48] B. Schoene, J. L. Crowley, D. J. Condon, M. D. Schmitz, and S. A. Bowring, "Reassessing the uranium decay constants for geochronology using ID-TIMS U–Pb data," *Geochim. Cosmochim. Acta*, vol. 70, no. 2, pp. 426–445, Jan. 2006, doi: 10.1016/j.gca.2005.09.007.

[49] J. Sláma *et al.*, "Plešovice zircon — A new natural reference material for U–Pb and Hf isotopic microanalysis," *Chem. Geol.*, vol. 249, no. 1–2, pp. 1–35, Mar. 2008.

[50] J. B. Paces and J. D. Miller, "Precise U-Pb ages of Duluth Complex and related mafic intrusions, northeastern Minnesota: Geochronological insights to physical, petrogenetic, paleomagnetic, and tectonomagmatic processes associated with the 1.1 Ga Midcontinent Rift System," *J. Geophys. Res. Solid Earth*, vol. 98, no. B8, pp. 13997–14013, Aug. 1993.

[51] S. Mansour, N. Hasebe, and A. Tamura, "Erosional reservoir for the northern segment of the Arabian-Nubian shield: Constrains from U-Pb geochronology of the lower palaeozoic succession, North Eastern Desert, Egypt," *Precambrian Res.*, vol. 388, p. 107017, May 2023.

[52] M. Guillong, A. Von Quadt, S. Sakata, I. Peytcheva, and O. Bachmann, "LA-ICP-MS Pb–U dating of young zircons from the Kos–Nisyros volcanic centre, SE Aegean arc," *J Anal Spectrom*, vol. 29, no. 6, pp. 963–970, 2014, doi: 10.1039/C4JA00009A.

[53] P. Vermeesch, "IsoplotR: A free and open toolbox for geochronology," *Geosci. Front.*, vol. 9, no. 5, pp. 1479–1493, Sep. 2018, doi: 10.1016/j.gsf.2018.04.001.

[54] D. Rubatto, "Zircon trace element geochemistry: partitioning with garnet and the link between U–Pb ages and metamorphism," *Chem. Geol.*, vol. 184, no. 1–2, pp. 123–138, Mar. 2002.

[55] D. Rubatto, "Zircon: the metamorphic mineral," pp. 261–295, 2017.

[56] R. J. Stern, K. A. Ali, J. P. Liegeois, P. R. Johnson, W. Kozdroj, and F. H. Kattan, "Distribution and significance of pre-Neoproterozoic zircons in juvenile Neoproterozoic igneous rocks of the Arabian-Nubian Shield," *Am. J. Sci.*, vol. 310, no. 9, pp. 791–811, Nov. 2010.

[57] K. A. Ali, S. A. Wilde, R. J. Stern, A.-K. M. Moghazi, and S. M. M. Ameen, "Hf isotopic composition of single zircons from Neoproterozoic arc volcanics and post-collision granites, Eastern Desert of Egypt: Implications for crustal growth and recycling in the Arabian-Nubian Shield," *Precambrian Res.*, vol. 239, pp. 42–55, Dec. 2013.